



Third European Conference on the Structural Integrity of Additively Manufactured Materials
(ESIAM23)

Tensile and nanoindentation tests analysis of Ti6Al4V alloy manufactured by laser powder bed fusion

David Liović^{a,*}, Marina Franulović^a, Nenad Gubeljak^b, Ervin Kamenar^{a,c}, Dražan Kozak^d,
Emanuele Vaglio^e

^aUniversity of Rijeka, Faculty of Engineering, Vukovarska 58, 51000 Rijeka, Croatia

^bUniversity of Maribor, Faculty of Mechanical Engineering, Smetanova ul. 17, 2000 Maribor, Slovenia

^cUniversity of Rijeka, Centre for Micro- and Nanosciences and Technologies, Laboratory for Precision Engineering and the Micro- and Nanosystems Technologies, 51000 Rijeka, Croatia

^dUniversity of Slavonski Brod, Mechanical Engineering Faculty in Slavonski Brod, Trg I.B. Mažuranić 2, 35000 Slavonski Brod, Croatia

^ePolytechnic Department of Engineering and Architecture, University of Udine, Via delle Scienze 206, 33100 Udine, Italy

Abstract

Additive manufacturing (AM) technologies are widely used in the fabrication of topologically complex components with thin-walled features, such as lattice structures. In this context, Laser Powder Bed Fusion (L-PBF) is one of the most commonly used AM technologies for producing such components. In order to further expand and justify the application of these components in operation and to model their mechanical behavior, it is necessary to know the mechanical properties of the matrix material from which they are formed. Therefore, there is currently a high interest in studying the behavior of these materials when subjected to monotonic or cyclic loading. However, determining the mechanical properties of the matrix material of thin-walled structures using tensile tests is challenging on the required subsize specimens. As a micro- or even nano-scale technology, nanoindentation can be used to probe a small volume of specimen, thus allowing the mechanical properties such as Young modulus, of thin-walled structures to be determined. In this work, Young's modulus of L-PBF Ti6Al4V alloy produced using different laser power and scanning speed combinations, has been determined on nano and macro scale. By comparing obtained results at both scales, it is evident that Young's modulus values determined at nano scale are higher and more scattered when compared to results determined at macro scale. Furthermore, this study implies that a wider range or a higher number of L-PBF process parameters should be considered to model its influence on Young's modulus with higher accuracy.

© 2023 The Authors. Published by Elsevier B.V.

This is an open access article under the CC BY-NC-ND license (<https://creativecommons.org/licenses/by-nc-nd/4.0>)

Peer-review under responsibility of the scientific committee of the ESIAM23 chairpersons

Keywords: Nanoindentation; tensile test; mechanical properties; L-PBF; Ti6Al4V alloy.

* Corresponding author. Tel.: +385 51 505700

E-mail address: dliovic@riteh.hr

1. Introduction

Laser powder bed fusion (L-PBF) proved to be effective technology for producing thin-walled and topologically complex products out of metallic materials such as: Ti6Al4V, AlSi10Mg, CoCr, 316L and Inconel 625 as shown by [Lvov et al. \(2023\)](#); [Arjunan et al. \(2020\)](#); [Limmahakhun et al. \(2017\)](#); [Platek et al. \(2020\)](#); [Leary et al. \(2018\)](#). These products have potential applications in the medical sector, as demonstrated by [Heinl et al. \(2007\)](#), as well as in the automotive and aeronautical industries, as highlighted by [Tabatabaei and Atluri \(2017\)](#). In order to confidently and reliably use these products in various applications, it is crucial to know how they behave when monotonic or cyclic load is applied. In such complex and low volume components, the reliable determination of mechanical properties of matrix material is challenging. If standardized specimens were used, the question is how reliable they represent the real component, given that they are often much thicker than the component itself while their shape may be different. [Roach et al. \(2020\)](#) have demonstrated that the mechanical properties of additively manufactured components can be influenced by both their size and shape, introducing additional complexity to the analysis. [Razavi et al. \(2020\)](#) proved that thickness influence mechanical properties under quasistatic and fatigue loading conditions. In addition, [Moura et al. \(2020\)](#) have reported that specimen's width and thickness have influence on fracture mode and associated micromechanisms of fracture. As stated by [Razavi et al. \(2020\)](#), the geometry and material characteristics of additively manufactured parts are related, meaning that any adjustment made to the part's geometry will trigger corresponding modifications in the underlying manufacturing process. In addition, if subsize or thin specimens are used to match the real component, it is challenging to perform tensile tests and reliably determine mechanical properties due to high deviations between measurements.

By using nanoindentation, the determination of mechanical properties of small volume specimens is possible. This opens up the possibility to perform tests on the low volume and topologically complex structures without producing subsize specimens for tensile tests. Using this method, it may become possible to avoid the difficulties associated with conducting reliable tensile tests on subsize specimens. However, nanoindentation is a sensitive method, and its results can be influenced by local microstructural heterogeneities as shown by [Chang et al. \(2021\)](#), thereby preventing a direct connection with the macroscopic behavior of components. Local heterogeneities are common for most metallic materials produced using PBF technologies, as demonstrated by [Hosseini and Popovich \(2019\)](#); [Donik et al. \(2020\)](#); [Dong et al. \(2020\)](#). On the other hand, microstructural features of additively manufactured Ti6Al4V alloy are significantly smaller than the Berkovich tip itself as demonstrated by [Liović et al. \(2023\)](#). In addition, [Dareh Baghi et al. \(2019\)](#) stated that nanoindentation method is suitable for the mechanical characterization of L-PBF Ti6Al4V alloy in the as-built state given that its microstructure is composed of single-phase grains.

The above mentioned findings opened up a possibility to use a nanoindentation method on L-PBF Ti6Al4V alloy and generalize measured results. In this way it may be possible to connect mechanical properties determined on nano scale to mechanical properties determined on macro scale. As stated by [Ter Haar and Becker \(2018\)](#), the annealing heat treatments when performed below critical temperature on L-PBF Ti6Al4V alloy cause formation of the α and β laths in the microstructure. In this way, by applying annealing heat treatment, the certain heterogeneity level is induced in the microstructure. However, [Cepeda-Jiménez et al. \(2020\)](#) have shown that the microstructure in that case is highly textured as well. In that case too, the microstructural features are still significantly smaller than the Berkovich tip itself, as discussed by [Liović et al. \(2023\)](#). Furthermore, [Cepeda-Jiménez et al. \(2020\)](#) have shown that application of different energy densities in L-PBF process through different process parameter combinations influence the microstructure. Using nanoindentation, it is possible to directly determine Young's modulus and hardness by analysing displacement and load data. Mechanical properties such as flow stress, indentation yield strength and creep resistance can be determined from nanoindentation load-unload curves, by applying already developed modeling techniques as shown by [Tuninetti et al. \(2021\)](#); [Weaver and Kalidindi \(2016\)](#); [Xu et al. \(2019b\)](#).

In this study, both tensile and nanoindentation tests were performed on Ti6Al4V specimens that had been produced using different L-PBF process parameters. Despite encountering numerous challenges while working with subsize specimens of the L-PBF Ti6Al4V alloy, the tensile tests were successfully conducted. Obtained results in terms of Young's modulus have been derived, compared and discussed both for tensile and nanoindentation tests. Furthermore, nonlinear regression models have been developed to relate Young's modulus values determined using tensile tests with laser power and scanning speed. In this way, the influence of the laser power and scanning speed on the Young's modulus has been analysed.

2. Materials and methods

A total of 27 tensile test and 9 cubic specimens were experimentally tested. The specimens were produced using Concept Laser M2 machine using three laser power levels (200, 225 and 250 W) combined with three scanning speed levels (1000, 1250 and 1500 mm/s). The laser power and scanning speed combinations were set according to face centered central composite design. The powder layer thickness, hatch distance and laser spot diameter were set to 0.025 mm, 0.09 mm and 0.1 mm, respectively. Both tensile and cubic specimens were manufactured using bi-directional single pass scanning strategy with 90° rotation of scan vector between layers. After manufacturing, the specimens were subjected to annealing heat treatment. The L-PBF and annealing heat treatment were conducted under argon atmosphere. During annealing heat treatment, specimens were held at the temperature of 840°C for 120 minutes, followed by cooling in furnace under argon atmosphere until the temperature of 150°C has been reached.

Tensile testing was conducted using an INSTRON 1255 – 8500 plus universal servo-hydraulic machine. This testing apparatus was equipped with two load cells, one with a capacity of 20 kN and the other with a capacity of 250 kN. The crosshead speed was consistently set to 0.01 mm/s throughout the entire elastic and plastic phases of the material's behavior. During the tensile tests, the strain fields were monitored using a GOM ARAMIS adjustable 2D/3D 12M system. The subsize tensile test specimen dimensions are shown in Fig. 1b. Given the high ultimate tensile strength of the L-PBF Ti6Al4V alloy, along with surface-bonded particles and a limited gripping area, conducting tensile tests became challenging due to the tendency of specimens to slipping. Additionally, when working with such small specimens, ensuring their precise alignment within the grips is crucial. To address these concerns, specially designed self-aligning grips were employed, effectively preventing specimen slippage and ensuring proper alignment.

Prior to nanoindentation, proper specimen preparation is essential to ensure the accuracy and reliability of measurements. To achieve this, cubic specimens (Fig. 1a) were embedded in resin, subjected to grinding using SiC papers, followed by a polishing process involving polycrystalline diamond paste. The final step in the preparation involved etching the specimens with Kroll's reagent (composed of 92% distilled water, 6% HNO₃, and 2% HF) for 20 seconds, followed by thorough rinsing with warm water.

All nanoindentation experiments were carried out using a Nano Indenter G200. These experiments were conducted at room temperature, using a three-sided Berkovich diamond indenter. To ensure precise and accurate measurements, great care was taken to maintain the drift during testing below 0.05 nm/s. This strict control over drift minimized the potential adverse effects of temperature variations on the measurement results. While calculating Young's modulus value, a Poisson's ratio of 0.33 has been used, which corresponds to the material properties of Ti6Al4V alloy, as stated by Xu et al. (2019a). The nanoindentation measurements have been performed using continuous stiffness measurement method. Before performing Young's modulus measurements, an analysis was conducted to assess location dependence. Additionally, the indentation depth interval for the evaluation of Young's modulus was adopted from Liović et al. (2023).

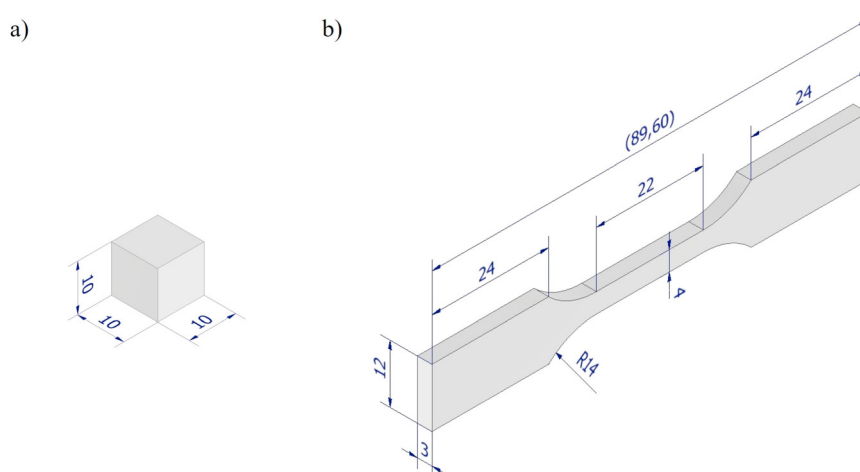


Fig. 1. (a) Dimensions of cubic specimens used for nanoindentation tests; (b) Dimensions of tensile test specimens.

The coefficients of full quadratic model have been found using Ordinary Least Square (OLS) method. Then, the second proposed regression model has been constructed by eliminating the nonsignificant model parameters while ensuring there is no statistically significant difference in model's fitting performance by using ANOVA procedure. Furthermore, the validity of the utilized OLS method has been checked using Non-constant Variance Score (NCV) and Shapiro-Wilk (S-W) tests. The NCV test has been applied to test whether the error variance changes with the level of the utilized predictors, while S-W test has been used to test normality of studentized residuals. The 95% confidence intervals for Young's modulus, the prediction variable in this case, have been determined using the following equation:

$$\mu_{y|x_0} = \hat{y}(x_0) \pm t_{\alpha/2,df(error)} \sqrt{\hat{\sigma}^2 \cdot \mathbf{x}_0'(\mathbf{X}'\mathbf{X})^{-1}\mathbf{x}_0}, \quad (1)$$

where $\hat{y}(x_0)$ represents the estimated mean response at the grid point, \mathbf{x}_0 is a vector containing grid points, \mathbf{X} is a model matrix formed by expanding the levels of the independent variables into their modeling form, $\hat{\sigma}^2$ is the estimated error variance, and $t_{\alpha/2,df(error)}$ denotes the t -value associated with the desired confidence level and the degrees of freedom of the residuals.

3. Results and discussion

As shown in Tab. 1, the mean Young's modulus values obtained using nanoindentation tests (E_{nano}) exceed those obtained through tensile testing (E_{tensile}). Young's modulus results determined using nanoindentation method are adapted from Liović et al. (2023). Notably, the coefficients of variations (CoV) for Young's modulus values derived from nanoindentation tests are consistently higher than those corresponding to tensile tests. This observation confirms that the nanoindentation method exhibits greater sensitivity to localized heterogeneities, resulting in increased data scatter. In the case of nanoindentation and tensile tests, the most significant differences between specimen groups in mean Young's modulus values are 16 GPa and 6.1 GPa, respectively. Thus, alternation of laser power and scanning speed in specified ranges, appears to be impractical to achieve a substantial change in Young's modulus that would be relevant for engineering applications.

Table 1. Young's modulus values determined using tensile and nanoindentation tests on different specimen groups.

P, W	$v, \text{ mm/s}$	$E_d, \text{ J/mm}^3$	ID	$E_{\text{nano}}, \text{ GPa}$	CoV, %	$E_{\text{tensile}}, \text{ GPa}$	CoV, %	Rel. diff., %
200	1000	88.9	A	126 (8)	6.3	109 (2)	1.8	15.6
	1250	71.1	B	129 (4)	3.3	108.9 (0.9)	0.8	18.5
	1500	59.3	C	129 (9)	6.7	109 (3)	2.8	18.3
225	1000	100	D	121 (8)	7.0	111.3 (0.6)	0.5	8.7
	1250	80	E	129 (6)	4.6	111 (1)	0.9	16.2
	1500	66.7	F	134 (1)	1.0	115 (1)	0.9	16.5
250	1000	111.1	G	137 (3)	2.0	109 (2)	1.8	25.7
	1250	88.9	H	131 (3)	1.9	113 (1)	0.9	15.9
	1500	74.1	I	128 (2)	1.3	110.3 (0.9)	0.8	16

Notes: All values are reported as: mean (standard deviation). E_{nano} results are adapted from Liović et al. (2023). Rel. diff. stands for relative difference.

It is worth noting that the highest difference in mean Young's modulus values determined by nanoindentation and tensile tests was observed within the G group of specimens (25.7%), which were produced using the highest energy density. As Cepeda-Jiménez et al. (2020) have stated, higher energy densities result in a more textured microstructure of L-PBF Ti6Al4V alloy. It seems that this more pronounced texture has a more pronounced influence on the Young's modulus values determined through the nanoindentation method compared to those obtained through tensile testing.

Young's modulus values of the Ti6Al4V alloy manufactured using different AM technologies and heat treatments are widely reported by Tevet et al. (2022); Szafrńska et al. (2019); Vrancken et al. (2012). However, the regression models which describe the influence of P and v on the Young's modulus of L-PBF Ti6Al4V alloy with high accuracy are thus far rarely reported. Within this framework, two regression models (M1 and M2) have been developed, statistically tested, compared to each other, and then analysed regarding their performance and complexity. By testing the models reported in Tab. 2 using ANOVA procedure, it was found that the model M1 does not have a significantly better fit than the model M2 (p -value = 0.223). More specifically, P is a more dominant predictor than v when

modelling of E_{tensile} is required. Both models have homoscedastic variance of error term tested using NCV test and normally distributed studentized residuals tested by S-W test (p – value > 0.05 in all cases).

Table 2. Regression models for the Young’s modulus and their statistical properties.

Model	E_{tensile}	R^2	Adj. R^2	p – value (NCV)	p – value (S-W)
M1	$E = -4.2604P^2 - 0.0055v^2 + 1856.7874P + 1.0876v + 0.071Pv - 1.02 \times 10^5$	0.453	0.322	0.793	0.212
M2	$E = 0.0585P^2 + 1.078 \times 10^5$	0.291	0.262	0.817	0.690

As can be seen in the Fig. 2, P has more dominant influence on the Young’s modulus, as the curvature of the response surface is more pronounced along P axis. This is confirmed through the results shown in Tab. 3, where the p -values for each model term were reported. As can be seen, only P^2 and intercept were significant model terms. However, the model has low R^2 value indicating that there might be other variables that should be considered when modeling the influence of L-PBF process parameter on E_{tensile} . Another approach to increase the R^2 might be to use higher number of laser power and scanning speed combinations chosen at wider parameter ranges. However, this could trigger different melting modes during L-PBF process led by different governing physical processes which in turn might be hard to describe using single regression model, as shown by Vaglio et al. (2023).

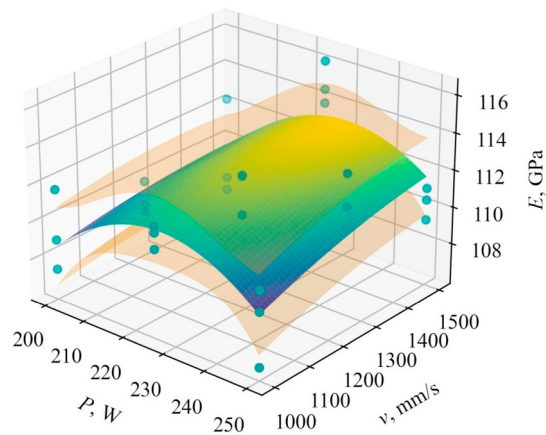


Fig. 2. Response surface with added 95% confidence intervals representing the influence of P and v on the E_{tensile} .

In this case, the regression models were reported only for E_{tensile} given that models developed for E_{nano} didn’t meet the requirement for homoscedastic variance of error term. In addition, developed models for E_{nano} had low R^2 and $adj. R^2$ values. The main reason for that is relatively large difference in data scatter for specific groups of specimens which can be seen in Tab. 1. For example, specimen F has standard deviation of 1 GPa, while specimen C has standard deviation of 9 GPa.

Table 3. Significance of full quadratic model parameters.

Source	p -value	Remark
Intercept	< 0.001	significant
P	0.14	not significant
v	0.10	not significant
P^2	0.003	significant
v^2	0.67	not significant
Pv	0.44	not significant

For a different applied heat treatments, Vrancken et al. (2012) reported Young's modulus values ranging from 112 ± 3.4 GPa to 115.5 ± 2.4 GPa. Hence, not even the applied heat treatments affect the Young's modulus values. The Young's modulus values reported in this study for annealed L-PBF Ti6Al4V alloy, produced using nine different combinations of P and v , closely align with those documented by Vrancken et al. (2012). Furthermore, by controlling P and v within the selected range in this study, it is evident that its impact on Young's modulus values at both macro and nano scales is relatively low. Hence, if specific Young's modulus values for the L-PBF components are required, then an integration of the unit cells with targeted sizes and types should be considered in the early product design phase.

4. Conclusions

The Young's modulus of the Ti6Al4V alloy produced using L-PBF was experimentally determined for nine different combinations of laser power and scanning speed, both on the nano and macro scales. Furthermore, this study considered the influence of laser power and scanning speed on Young's modulus values at both scales. These findings are applicable to L-PBF Ti6Al4V alloy manufacturing processes employing laser power settings ranging from 200 W to 250 W and scanning speeds ranging from 1000 mm/s to 1500 mm/s. The Young's modulus values obtained through nanoindentation were found to be higher, along with their coefficients of variations, in comparison to those obtained through tensile tests. The highest difference between mean Young's modulus values determined using two methods were observed in specimens produced using the highest energy density value. However, it is worth noting that the differences in measured Young's modulus values, especially at macro scale, are of minor magnitude to be considered significant for engineering applications. A relatively low R^2 value of 0.453 imply that a wider range of parameters with more combinations should be considered, or additional variables relevant to the L-PBF process should be included as predictors.

In future work, elastoplastic material properties will be calibrated using the experimentally acquired load-displacement curve. This calibration process will rely on computational modeling procedures, wherein the necessary model parameters will be obtained either through the finite element method or extracted from the experimentally recorded load-displacement curves.

Acknowledgements

This research has received support from the Croatian Science Foundation under project number IP-2019-04-3607 and from the University of Rijeka under project number uniri-tehnic-18-34. Furthermore, a portion of this work was made possible through access to equipment acquired under the ERDF project RC.2.2.06-0001 "RISK." Additionally, some of the research presented in this study was supported by the Research program P2-0137, titled "Numerical and experimental analysis of mechanical systems," funded by the Slovenian Research Agency-ARRS. Emanuele Vaglio is grateful for funding under the REACT EU Italian PON 2014-2020 Program - Action IV.4 - Innovation (DM 1062, 10/08/2021).

References

- Arjunan, A., Singh, M., Baroutaji, A., Wang, C., 2020. Additively manufactured AlSi10Mg inherently stable thin and thick-walled lattice with negative Poisson's ratio. *Composite Structures* 247, 112469.
- Cepeda-Jiménez, C.M., Potenza, F., Magalini, E., Luchin, V., Molinari, A., Pérez-Prado, M.T., 2020. Effect of energy density on the microstructure and texture evolution of Ti-6Al-4V manufactured by laser powder bed fusion. *Materials Characterization* 163, 110238.
- Chang, Y., Lin, M., Hangen, U., Richter, S., Haase, C., Bleck, W., 2021. Revealing the relation between microstructural heterogeneities and local mechanical properties of complex-phase steel by correlative electron microscopy and nanoindentation characterization. *Materials & Design* 203, 109620.
- Dareh Baghi, A., Ghomashchi, R., Oskouei, R.H., Ebandorff-Heidepriem, H., 2019. Nano-mechanical Characterization of SLM-Fabricated Ti6Al4V Alloy: Etching and Precision. *Metallography, Microstructure, and Analysis* 8, 749–756.
- Dong, Z., Liu, Y., Zhang, Q., Ge, J., Ji, S., Li, W., Liang, J., 2020. Microstructural heterogeneity of alsi10mg alloy lattice structures fabricated by selective laser melting: Phenomena and mechanism. *Journal of Alloys and Compounds* 833, 155071.
- Donik, Č., Kraner, J., Paulin, I., Godec, M., 2020. Influence of the energy density for selective laser melting on the microstructure and mechanical properties of stainless steel. *Metals* 10, 1–19.

- Heinl, P., Rottmair, A., Körner, C., Singer, R.F., 2007. Cellular titanium by selective electron beam melting. *Advanced Engineering Materials* 9, 360–364.
- Hosseini, E., Popovich, V., 2019. A review of mechanical properties of additively manufactured inconel 718. *Additive Manufacturing* 30, 100877.
- Leary, M., Mazur, M., Williams, H., Yang, E., Alghamdi, A., Lozanovski, B., Zhang, X., Shidid, D., Farahbod-Sternahl, L., Witt, G., Kelbassa, I., Choong, P., Qian, M., Brandt, M., 2018. Inconel 625 lattice structures manufactured by selective laser melting (SLM): Mechanical properties, deformation and failure modes. *Materials and Design* 157, 179–199.
- Limmahakhun, S., Oloyede, A., Sithiseripratip, K., Xiao, Y., Yan, C., 2017. Stiffness and strength tailoring of cobalt chromium graded cellular structures for stress-shielding reduction. *Materials and Design* 114, 633–641.
- Liović, D., Franulović, M., Kamenar, E., Kozak, D., 2023. Nano-Mechanical Behavior of Ti6Al4V Alloy Manufactured Using Laser Powder Bed Fusion. *Materials* 16, 4341.
- Lvov, V.A., Senatov, F.S., Shinkaryov, A.S., Chernyshikhin, S.V., Gromov, A.A., Sheremetyev, V.A., 2023. Experimental 3D printed re-entrant auxetic and honeycomb spinal cages based on Ti-6Al-4 V: Computer-Aided design concept and mechanical characterization. *Composite Structures* 310, 116766.
- Moura, L.S., Vittoria, G.D., Gabriel, A.H., Fonseca, E.B., Gabriel, L.P., Webster, T.J., Lopes, É.S., 2020. A highly accurate methodology for the prediction and correlation of mechanical properties based on the slimmness ratio of additively manufactured tensile test specimens. *Journal of Materials Science* 55, 9578–9596.
- Platek, P., Sienkiewicz, J., Janiszewski, J., Jiang, F., 2020. Investigations on mechanical properties of lattice structures with different values of relative density made from 316L by selective laser melting (SLM). *Materials* 13.
- Razavi, N., Van Hooreweder, B., Berto, F., 2020. Effect of build thickness and geometry on quasi-static and fatigue behavior of Ti-6Al-4V produced by Electron Beam Melting. *Additive Manufacturing* 36, 101426.
- Roach, A.M., White, B.C., Garland, A., Jared, B.H., Carroll, J.D., Boyce, B.L., 2020. Size-dependent stochastic tensile properties in additively manufactured 316L stainless steel. *Additive Manufacturing* 32, 101090.
- Szafrańska, A., Antolak-Dudka, A., Baranowski, P., Bogusz, P., Zasada, D., Małachowski, J., Czujko, T., 2019. Identification of Mechanical Properties for Titanium Alloy Ti-6Al-4V Produced Using LENS Technology. *Materials* 12, 886.
- Tabatabaei, M., Atluri, S.N., 2017. Simple and efficient analyses of micro-architected cellular elastic-plastic materials with tubular members. *International Journal of Plasticity* 99, 186–220.
- Ter Haar, G.M., Becker, T.H., 2018. Selective laser melting produced Ti-6Al-4V: Post-process heat treatments to achieve superior tensile properties. *Materials* 11.
- Tevet, O., Svetlizky, D., Harel, D., Barkay, Z., Geva, D., Eliaz, N., 2022. Measurement of the Anisotropic Dynamic Elastic Constants of Additive Manufactured and Wrought Ti6Al4V Alloys. *Materials* 15, 638.
- Tuninetti, V., Jaramillo, A.F., Riu, G., Rojas-Ulloa, C., Znaidi, A., Medina, C., Mateo, A.M., Roa, J.J., 2021. Experimental Correlation of Mechanical Properties of the Ti-6Al-4V Alloy at Different Length Scales. *Metals* 11, 104.
- Vaglio, E., Totis, G., Lanzutti, A., Fedrizzi, L., Sortino, M., 2023. A novel thermo-geometrical model for accurate keyhole porosity prediction in Laser Powder-Bed Fusion. *Progress in Additive Manufacturing* .
- Vrancken, B., Thijs, L., Kruth, J.P., Van Humbeeck, J., 2012. Heat treatment of Ti6Al4V produced by Selective Laser Melting: Microstructure and mechanical properties. *Journal of Alloys and Compounds* 541, 177–185.
- Weaver, J.S., Kalidindi, S.R., 2016. Mechanical characterization of Ti-6Al-4V titanium alloy at multiple length scales using spherical indentation stress-strain measurements. *Materials and Design* 111, 463–472.
- Xu, Y., Zhang, D., Hu, S., Chen, R., Gu, Y., Kong, X., Tao, J., Jiang, Y., 2019a. Mechanical properties tailoring of topology optimized and selective laser melting fabricated Ti6Al4V lattice structure. *Journal of the Mechanical Behavior of Biomedical Materials* 99, 225–239.
- Xu, Z., Zhang, H., Li, W., Mao, A., Wang, L., Song, G., He, Y., 2019b. Microstructure and nanoindentation creep behavior of CoCrFeMnNi high-entropy alloy fabricated by selective laser melting. *Additive Manufacturing* 28, 766–771.